Astronomy & Astrophysics manuscript no. USS0943
March 13, 2015

The Mysterious Morphology of MRC0943-242

B. Gullberg[1] et al.

European Southern Observatory, Karl-Schwarzschild-Str. 2, D-85748 Garching
e-mail: bgullber@eso.org

?

ABSTRACT

We here present a pilot study of the HzRG USS0943-242 at $z = 2.923$ where we for the first time combine ALMA and MUSE data cubes. Using these 3D data cubes we disentangle the AGN and starburst dominated components of the systems, and reveal a highly complex morphology, as the AGN, starburst and molecular gas components show up as widely separated sources in dust continuum, optical continuum and CO line emission observations. CO(1–0) and CO(8–7) line emission suggest a molecular gas reservoir, offset from both the dust and optical continuum.

Key words. ? – ? – ?

1. Introduction

High-z radio galaxies (HzRGs = $L_{3\,GHz} > 1026\,\mathrm{W\,Hz^{-1}}$ and $z > 1$) are unique markers of the most powerful galaxies in the early Universe, showing signatures of both powerful AGN activity and extreme starbursts. HzRGs are some of the most massive galaxies known at any redshift, with $M > 10^{11}\,\mathrm{M_\odot}$ of stars (Seymour et al. 2007; De Breuck et al. 2010) confirming prior indications from the tight correlation of the observed near-IR Hubble K-z diagram for powerful radio sources (Lilly & Longair 1984; Eales et al. 1997; De Breuck et al. 2002). Given that stellar bulge mass correlates with black hole mass (e.g. Tremaine et al. 2002), it is no surprise that the most powerful radio galaxies reside in the most massive stellar hosts.

HzRGs are extremely luminous in both the mid-IR (Ogle et al. 2006; Seymour et al. 2007; De Breuck et al. 2010) and the sub-mm waveband (Archibald et al. 2001; Reuland et al. 2004). This has been interpreted as evidence of high black hole accretion rates combined with high star-formation rates (SFRs). The disentanglement of the AGN and starburst components requires excellent sampling of the spectral energy distribution (SED). Examples of this have been seen before: Seymour et al. (2012) illustrate the decomposition of the starburst and AGN components using 3.5 – 850 μm photometry in the $z = 2.16$ radio galaxy, PKS 1138-262, showing that both have roughly equal contributions to the IR luminosity. Ivison et al. (2012) present a detailed study of two $z > 3$ radio galaxies, including interferometric imaging of the CO(1–0) and CO(4–3) from JVLA and IRAM Plateau de Bure. In the cases of 4C41.17 (De Breuck et al. 2005) and 4C60.07 (Ivison et al. 2008) both at $z = 3.8$, two gas-rich components are found to be separated by ∼30 kpc, and the radio galaxy TXS0828+193 at $z = 2.6$ shows an even more widely separated (80 kpc) system (Nesvadba et al. 2009). In several of these systems, most of the gas and dust emission originates from the companion rather than the AGN host galaxy, while others (e.g. TXS0828+193) show no evidence for a companion in the deep *Spitzer* imaging.

Disentangling the SED of HzRG is the main goal of our HErschel Radio Galaxy Evolution (HERGÉ) project. The 71 HzRG targeted in the HERGÉ project are uniformly distributed across $1.0 < z < 5.2$ with a range of radio powers. This representative sample has recently obtained 5-band (70 to 500 μm) imaging, which adds to the SCUBA/LABOCA 850 μm photometry and 6-band *Spitzer* IR data (3.6 to 24 μm), used to determine host galaxy stellar masses and mid-IR AGN luminosities, Seymour et al. (2007); De Breuck et al. (2010).

Spitzer, Herschel, SCUBA and LABOCA data suggest that the sources targeted in the HERGÉ project have very high far-IR (FIR) luminosities (∼ $10^{13}\,\mathrm{L_\odot}$, Drouart et al. 2014), but the data do not have high enough spatial resolution to pinpoint the AGN host galaxies as the source of the FIR emission. However, the spatial resolution of ALMA cycle 1 data reveals a much more complex composition of AGN and starburst dominated sources than previously thought. We illustrate this by a pilot study of USS0943-242 (here after Yggdrasil) at $z = 2.9$, where we combine - for the first time - sensitive ALMA 235 GHz observations with VLT/MUSE Lyα and HeII observations.

This ultra steep spectrum source has a spectral index of $\alpha = -1.5$ between 1.4−30 GHz and shows no evidence of a spectral curvature within this range (Carilli et al. 1997; Emonts et al. 2011). Yggdrasil is located in a proto cluster and surrounded by many nearby companions detected in Lyα and with known redshifts (Venemans et al. 2007) and is surrounded by a giant quiescent Lyα halo with a diameter of ≥ 100 kpc - extending beyond the radio structure (Villar-Martín et al. 2003). A deep absorption trough in the Lyα emission line reveals the presence of a large amount of neutral gas on the line of sight of the HzRG (Binette et al. 2000; Jarvis et al. 2003).

In § 2 we present our ALMA sub-millimetre (submm) and MUSE optical observations. The results of these observations are given in § 3 and is analysed and discussed in § 4 and § 5. In § 6 we conclude.

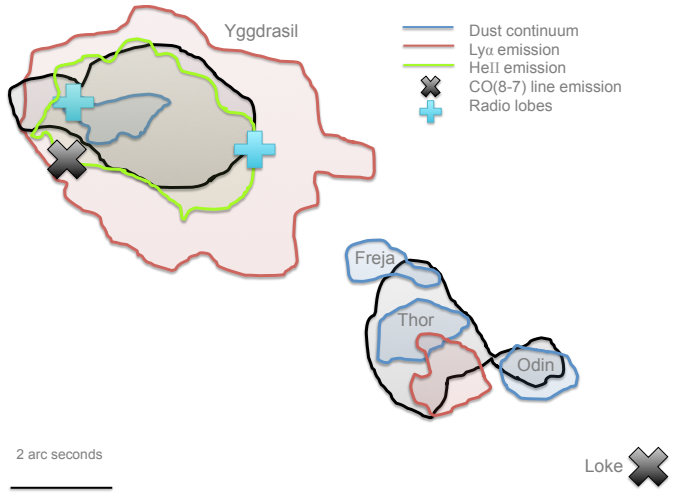

Fig. 1. Sketch of the complex morphology.

2. Observations

2.1. ALMA observations

The ALMA cycle 1 observations in Band 6 were carried out on 2014 April 29th for 3 min on-source time with 36 working antennas. Using the four 1 GHz bands to cover the frequency ranges 233.6 – 237.1 GHz and 248.6 – 252.3 GHz. We use the Common Astronomy Software Applications (CASA) and the supplied calibration script to calibrate the data and combine the four bands for image. In order to search for CO(8–7) line emission, which is within the frequency range at $z = 2.923$, we subtract the continuum in the UV-plane. As the dust continuum is not spatially resolved, we imaging the data with a full natural weighting (robust parameter of 2) to get as high signal to noise as possible. This results in a $0.7'' \times 0.6''$ beam with pa = 75.1° and an RMS of 0.1 mJy for the continuum. The line data is binned to 10 km/s and Hanning smoothed to XX km/s, and has an RMS of 1.7 mJy.

2.2. MUSE observations

MUSE (Bacon et al. 2010) observations were obtained on 2014 February 21st, during the first commissioning run of the instrument (see Bacon et al. 2014). This one hour observation taken under $\sim 1''$ seeing was split into three 20 min exposures taken at 45, 135 and 225 degree position angle with a small dithering offset to minimise the effect of systematics. In order to reach the Lyα line of Yggdrasil at 476.5 nm, we used the extended wavelength range mode (i.e. without second order blocking filter allowing to reach down to 465 nm). All data were processed with the version 1.0 of the MUSE pipeline (Weilbacher et al. 2012) to produce a fully calibrated and sky subtracted data cube. Finally, the cube was cleaned for sky subtraction residuals with the Principal Component Analysis (PCA) based algorithm ZAP developed by Soto et al (in prep.).

3. Results

Combining for the first time ALMA submm observations with MUSE optical observations reveals an even more complex morphology then seen at first: the star formation does not occur in the AGN host galaxy (Yggdrasil), but rather in a set of widely separated companions (Odin, Thor and Freja) connected by a bridge of Lyα emission (see Fig. 1).

3.1. Yggdrasil

The AGN dominated component - Yggdrasil - shows up both in the ALMA submm observations and in the MUSE optical observations. The MUSE observations show both strong Lyα(λ1215.7 Å), CIV (λ1550.8 Å) and HeII (λ1640.4 Å) emission, at the position of the AGN (see Fig 2). Due to Lyα and CIV both being resonant emission lines they are both subject to resonant scattering with in the emitting medium and absorption by neutral gas on the line of sight. This shows up as a deep absorption trough in the Lyα emission line. By centring the Lyα velocity profile at the HeII redshift of $z = 2.923$ the bottom of the absorption trough is at ~ -370 km/s. The two absorption troughs seen in the CIV emission line are due to the CIV doublet at $\lambda\lambda$1548.2, 1550.8 Å. As HeII is a fine structure emission line it does not show any sign of absorption by neural gas. Fitting single Gaussians to each of the three emission line velocity profiles yield a FWHM ranging from 1240-1490 km/s and integrating with in a 3σ width gives an integrated flux given in Table 1.

At the location of Yggdrasil we observe weak dust continuum emission at 235 GHz which summed over the region in CASA gives the flux density of 24.7 ± 0.2 mJy (see Table 1). In the ALMA data cube we detect CO(8–7) line emission at the 3σ level at the position of Yggdrasil (see Fig 3). The CO(8–7) emission line is only shifted with $\sim +50$ km/s from the HeII systemic redshift and fitting a single Gaussian to this narrow velocity profile yields a FWHM of 57 ± 12 km/s and integrating within 3σ yields and integrated line flux of 1.96 ± 0.13 Jy km/s.

IRAC: compact, bright, AGN host with M_*=XX seymour07+debreuck10

3.2. Odin, Thor and Freja

The ALMA 235 GHz continuum observations reveal three aligned starburst components (Freja, Odin and Thor) on a string shifted between $\sim 48 - 65$ kpc towards the South-West (SW) relative to the position of Yggdrasil (see Fig 1). Summing over the Odin, Thor and Freja regions in CASA we find the flux densities listed in Table 1.

Odin and Thor are the two brightest components. In-between these, we observe Lyα emission with MUSE (see Fig 2). Like the Lyα spectrum for Yggdrasil, the spectrum here also reveals the presence of a neutral gas reservoir by an absorption trough at the same velocity offset (see Fig 2). The peak intensity of this Lyα component is $\sim$ 18 times lower and the FWHM $\sim$ 3 times smaller than for the Lyα detection of Yggdrasil (see Table 1). However the two Lyα detections and the presence of an absorber at the same velocity offset in both, link Odin, Thor and Freja to Yggdrasil.

IRAC:diffuse emission

3.3. Loke

At a distance of $\sim$ 86 kpc from Yggdrasil we detect a component of CO(8–7) line emitting gas (Loke, see Fig. 1 and 3). Surprisingly Loke is not detected in any dust continuum nor optical counter parts. As for the CO(8–7) line detected at the position of Yggdrasil, the CO(8–7) lines is narrow with FWHM = 74 ± 13 km/s, only shifted by $\sim$ 50 km/s from the HeII systemic redshift, and peaks at the same intensity. Searching the archival Australian Telescope Compact Array (ATCA) data for Yggdrasil

Component	Position		$S_{235\,\mathrm{GHz}}$	$S\,dV_{\mathrm{Ly}\alpha}$	$S\,dV_{\mathrm{HeII}}$	$S\,dV_{\mathrm{CIV}}$	$S\,dV_{\mathrm{CO(8-7)}}$
	RA	dec	mJy	mJy km/s	mJy km/s	mJy km/s	mJy km/s
Yggdrasil	09:45:32.769	-24.28.49.29	24.7 ± 0.2	94.13 ± 0.47	24.14 ± 0.35	26.52 ± 0.37	196.35 ± 12.73
Odin	09:45:32.222	-24.28.55.06	61.0 ± 0.7	2.33 ± 0.08	—	—	—
Thor	09:45:32.386	-24.28.54.05	66.5 ± 0.6		—	—	—
Freja	09:45:32.445	-24.28.52.55	21.2 ± 0.3		—	—	—
Loke	09:45:32.072	-24.28.56.94	<XX	—	—	—	231.42 ± 10.50

Table 1.

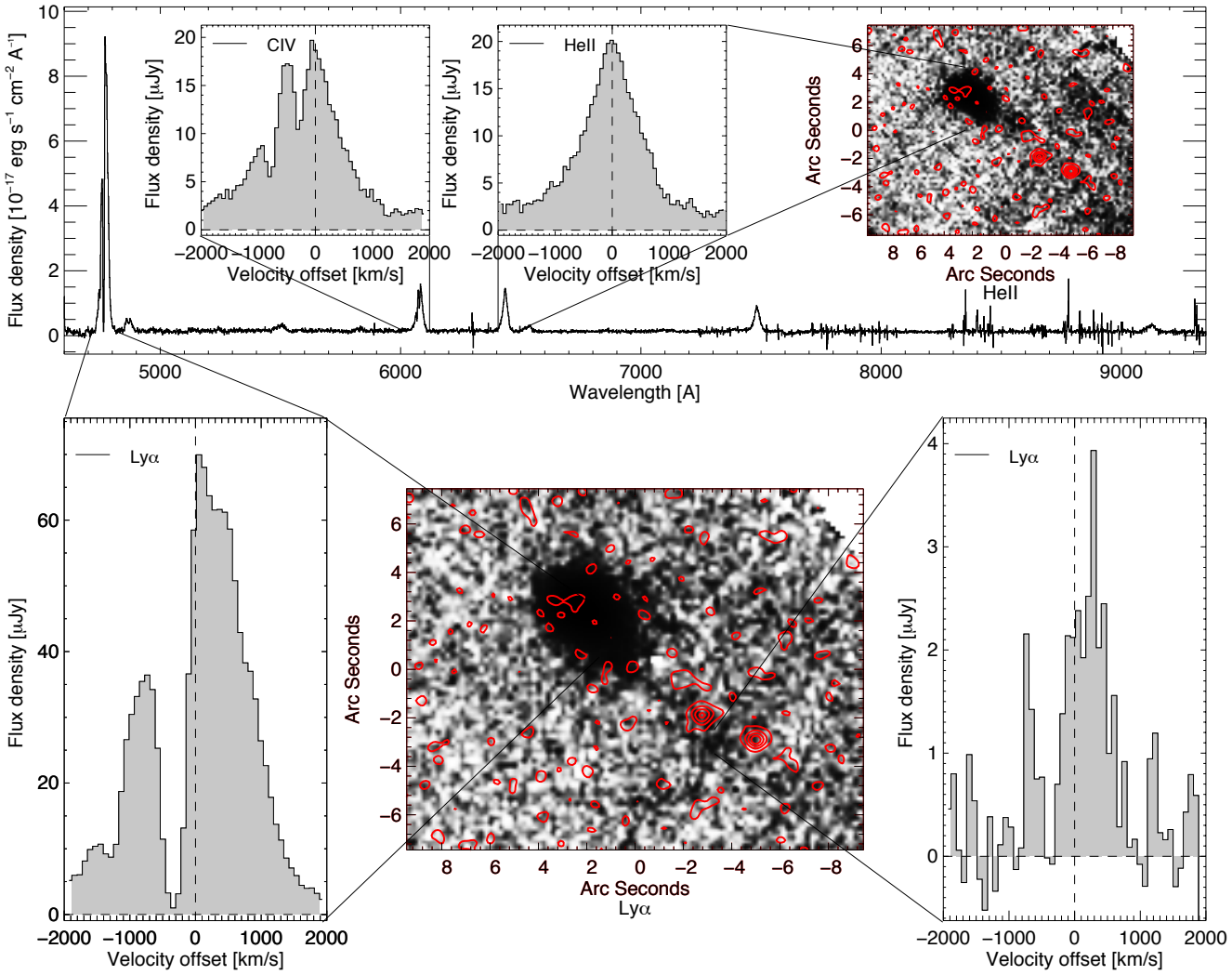

Fig. 2. The result of the MUSE observations revealing Lyα emission at the location of Yggdrasil and in-between Thor and Odin. The top panel shows the full MUSE spectrum extracted from the position of Yggdrasil with the aperture with a diameter of 2". The HeII and CIV velocity profiles are showed as zoom ins. At the right in the top panel the HeII emission is additionally show in grey scale and overlaid with the ALMA dust continuum contours in red. In the bottom panel is to the left a zoom in of the Lyα emission line from Yggdrasil. In the middle panel the Lyα emission is show in grey scale overlaid with the ALMA dust continuum contours in red and to the right is the Lyα velocity profile for the emission in-between Thor and Odin.

(see Emonts et al. 2011 for more detains), we find CO(1–0) line emission at the position of Loke (see Fig. 3), thereby confirming the existence of a large molecular gas reservoir. The detection of CO(1–0) emission and the CO(8–7) to CO(1–0) brightness temperature ratio of ~ 0.03 imply the presence of a low excited molecular gas reservoir. compare with thermal Unfortunately the ATCA observations are limited by the large beam and low signal to noise ratio, and can therefore not distinguish if the CO(1–0) emission originates from the dust continuum sources, a free molecular gas component in the halo or both. More observations with higher spatial resolution are required to make any further conclusion.

4. Analysis

4.1. Disentangling the SED

Yggdrasil has a well sampled spectral energy distribution (SED) with IRAC, MIPS, SPIRE (250 μm, 350 μm and 500 μm) and PACS (24 μm, 100 μm and 160 μm) from previous studies (De Breuck et al. 2010; Drouart et al. 2014). Reanalysing the PACS

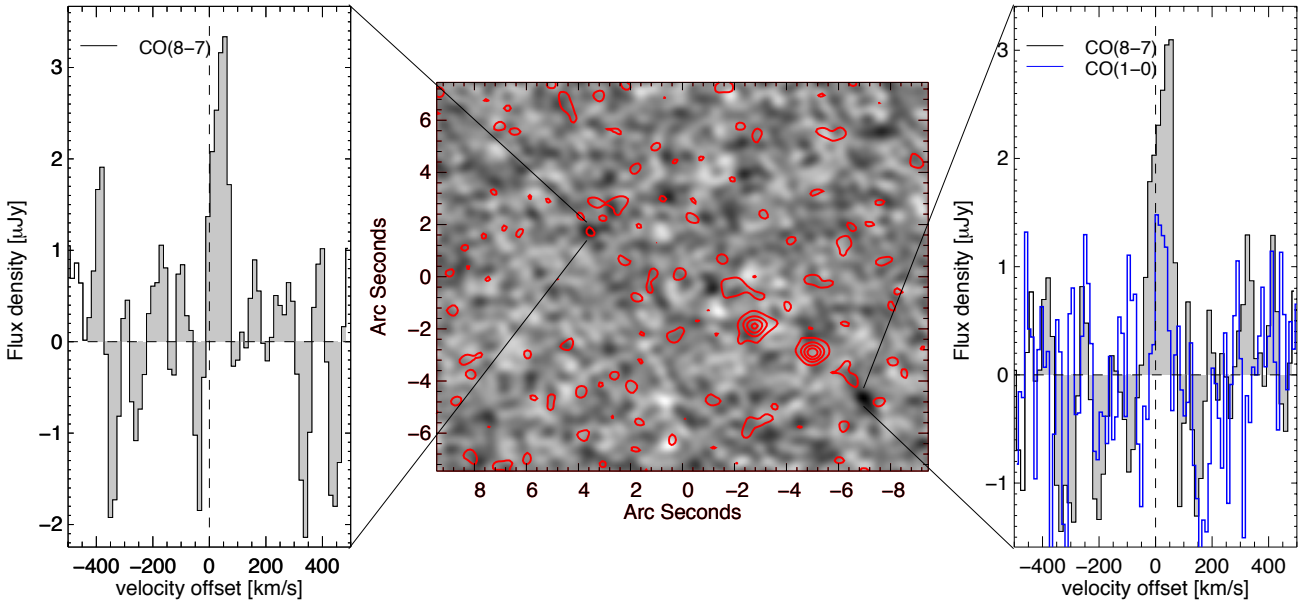

Fig. 3. The ALMA cube show CO(8–7) emission at two positions in the data cube: at the location of Yggdrasil and to the South-West in an isolated component: Loke. In the middle is the grey scale of the CO(8–7) emission overlaid with the ALMA dust continuum contours. To the left and right are plotted the CO(8–7) velocity profiles for both Yggdrasil (left) and Loke (rigth). Surprisingly the CO(8–7) lines only have a small offset from the HeII systemic redshift.

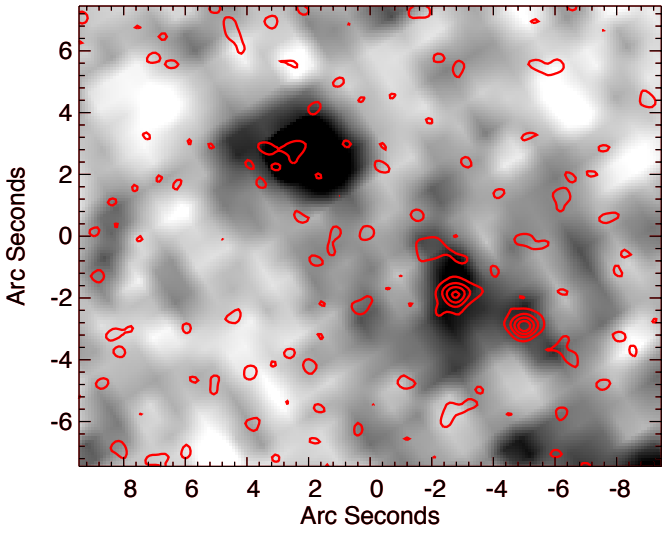

Fig. 4. In grey scale is the IRAC2 image and in red contours the ALMA dust continuum emission.

PACS - separation of the two components in the SED
SFR

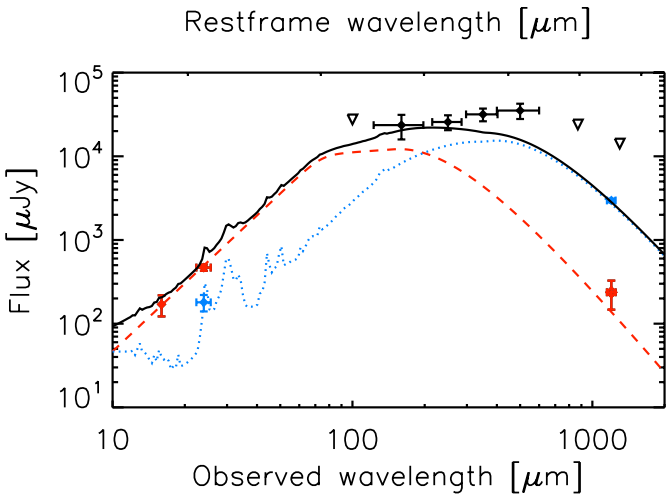

Fig. 5. The spectral energy distribution of USS0943-242. The spatial resolution of the ALMA data allow us to disentangle the SED in the AGN heated component (red curve) and star formation heated component (blue curve). The sum of these two components are illustrated by the black curve.

160 μm photometric data reveals an elongated source, spanning from the position of the Yggdrasil towards Odin, Thor and Freja. Likewise when returning to the IRAC imaging multiple components show up corresponding to Yggdrasil, Odin, Thor and Freja. However the noise of both the PACS and IRAC images are to high to disentangle the SED at these wavelengths. However, the high spatial resolution of the ALMA data allow us to disentangled the AGN and star formation heated components in the SED at 235 GHz. The very faint dust continuum emission detected in the AGN host galaxy is consistent with the Rayleigh-Jeans tail of AGN heated dust emission, putting an upper limit of $\sim 100\,M_{\odot}$/yr on the ongoing SFR (see Fig. 5).

5. Dicussion

5.1. Origin of morphology

The result from the disentanglement of the SED suggest that the starburst activity in HzRGs is driven by the interaction of two (or more) gas-rich systems. Major mergers have been invoked to explain the high star-formation rates seen in submm galaxies (SMGs; Engel et al. e.g. 2010), though others argue that they may rather represent the top end of a "main sequence'" of

HzRG	z	CO detection	separation	ref
MRC0114-211	1.402	CO(1–0)	30 kpc	Emonts et al. (2014)
MRC0152-209	1.921	CO(6–5)	10 kpc	Emonts et al. submitted.
MRC0156-252	2.016	CO(1–0)	10 kpc	Emonts et al. (2014)
MRC2048-272	2.060	CO(1–0)	40 kpc	Emonts et al. (2014)
MRC1138-26	2.161	CO(1–0)	30-40 kpc	Emonts et al. (2013)
TXS0828+193	2.572	CO(3–2)	80 kpc	Nesvadba et al. (2009)
MRC0943-242	2.923	CO(8–7)	80 kpc	this work
B3J2330+3927	3.086	CO(1–0)/CO(4–3)	30 kpc	Ivison et al. (2012)
4C41.172	3.798	CO(4–3)	13 kpc	De Breuck et al. (2005)
4C60.07	3.8	CO(1–0)/CO(4–3)	30 kpc	Ivison et al. (2008); Greve et al. (2004)

Table 2.

star-forming galaxies (Michałowski et al. 2012, e.g.). The similar morphologies and stellar masses of HzRGs and SMGs suggests they may be related, potentially through an evolutionary sequence, a high-z extension of the local relation between QSOs and ULIRGs (Sanders et al. 1988). Both classes reside in parent halos of similar mass (Hickox et al. 2012), but direct observations of objects in transition between SMGs and QSOs remain restricted to a few examples (Simpson et al. 2012, e.g.). This is where detailed observational studies of type 2 AGN like HzRGs can play an important role, as their stellar masses, unlike type 1 AGN's, can be accurately determined (Seymour et al. 2007; De Breuck et al. 2010) from *Spitzer* data.

The multi component system with an AGN dominated component and a starburst component connected by a bridge of Lyα emission, illustrate the complex morphology of HzRG. Ivison et al. (2008) observe multiple component for the HzRG 4C60.07 at $z = 3.8$, likewise connected by a bridge of gas. They interpret this bridge as a plume of cold dust and gas in a tidal steam between to interacting galaxies. The interaction between the two galaxies is believed to be the trigger of the starburst and therewith the exhaust of the molecular gas supply in the AGN host galaxy. One scenario which could have triggered the high star formation in Odin, Thor and Freja and perhaps the AGN activity in Yggdrasilis, like for 4C60.07, interaction between two galaxies. In this scenario the two galaxies move through each other triggering AGN activity in Yggdrasil, and pulls out the star forming gas leaving behind a tidal tail of Lyα emitting gas. The star formation then ignites in a sting of component Odin, Thor and Freja resulting in a SFR $\sim 1000\,M_\odot$/yr. However the narrow CO(8–7) show no sign of dynamical motion in either Yggdrasil or Loke. This makes it difficult to explain the morphology by galaxy-galaxy interaction or major merger, but instead suggest steady accretion of cold gas or a free molecular gas region in the halo environment.

5.2. Molecular gas reservoir

We find CO(8–7) emission in Loke which is not detected in any optical or dust continuum counterpart. It is not the first time CO line emission has been detected for Yggdrasil with out any counterpart at other frequencies/wavelengths. Emonts et al. (2011) discovered a tentative 3σ CO(1–0) detection spread over an area the size of the beam ~ 60 kpc North-East of Yggdrasil. This tentative detection has a line luminosity of $L'_{\rm CO(1-0)} \sim 8 \times 10^{10}\,{\rm K\,km\,s^{-1}\,pc^{-2}}$. Choosing $\alpha_{\rm CO} = 0.8\,M_\odot\,{\rm K\,km\,s^{-1}\,pc^{-2}}$ (Downes & Solomon 1998) Emonts et al. (2011) estimate a molecular gas mass of $M_{\rm H_2} = 6 \times 10^{10}\,M_\odot$. The detection of CO(1–0) at the position of Loke further confirms the presence of a large reservoir of molecular gas. However it is not clear from the observations at hand the extent of this reservoir, if it reaches across Odin, Thor and Freja and Loke therefore is tracing one compact region within the component or the reservoir is only at the location of Loke. Only future CO(1–0) observations with high spatial resolution will be able to reveal the extent of the diffuse molecular gas.

The misalignment of CO emission with the position of the HzRG is seen before in a few sources e.g. 4C60.07 (Ivison et al. 2008). Ivison et al. (2008) detect narrow CO(4–3) emission for the HzRG at $z = 3.8$ at two positions: at the location of the AGN core and 7" South-West of the AGN. The latter component is also detected in CO(1–0) emission (Greve et al. 2004). Based on the submm observations of 4C60.07, Ivison et al. (2008) point out a complication when calculating dynamical masses using the extended CO emission, due to the misalignment of the black hole with the CO emission and dust continuum. The submm and optical observations of Yggdrasil, makes this complication even clearer, with many components, with only two traced by CO emission.

Table 2: examples of misalignment/displacements

6. Conclusions

The spatial separation but simultaneous AGN and star formation activity of the radio-loud AGN Yggdrasil (aka USS0943-242) illustrate the complex morphology of HzRGs. Peculiarly, the star formation takes place $\sim 45 - 68$ kpc from the AGN in three aligned components. Even more surprisingly about Yggdrasil is the discovery of a molecular gas reservoir align with but beyond the star forming regions, not detected in any dust or optical counterparts. Yggdrasil is therefore the ideal source to use as a laboratory, for studying the complex morphology and processes taking place in HzRGs. It allows us to study AGN activity, star formation, winds and feedback and the influence of these on the surrounding medium. Based on these observations we can conclude that

1. The star formation and the AGN activity is not co-spatial, but simultaneous.
2. The combination of 3D data cubes are essential to understand the composition and morphology of HzRGs.
3. ...

This complexity of the morphology of Yggdrasil raises more questions than it answers: *Why do the AGN activity and star formation take place at the same time but in widely separated components? What interaction does the two components have? What is the connection between the starburst component and the*

molecular gas region? is the molecular gas being expelled or is it rather fuelling the star formation?

Only future studies of Yggdrasil and other HzRGs by combining 3D data cubes, can shed new light on the origin of the complex morphology of HzRGs.

Acknowledgements. ALMA + MUSE prog. ID

References

Archibald, E. N., Dunlop, J. S., Hughes, D. H., et al. 2001, MNRAS, 323, 417
Bacon, R., Accardo, M., Adjali, L., et al. 2010, in Society of Photo-Optical Instrumentation Engineers (SPIE) Conference Series, Vol. 7735, Society of Photo-Optical Instrumentation Engineers (SPIE) Conference Series, 8
Bacon, R., Vernet, J., Borisova, E., et al. 2014, The Messenger, 157, 13
Binette, L., Kurk, J. D., Villar-Martín, M., & Röttgering, H. J. A. 2000, A&A, 356, 23
Carilli, C. L., Röttgering, H. J. A., van Ojik, R., et al. 1997, ApJS, 109, 1
De Breuck, C., Downes, D., Neri, R., et al. 2005, A&A, 430, L1
De Breuck, C., Neri, R., Morganti, R., et al. 2003, A&A, 401, 911
De Breuck, C., Seymour, N., Stern, D., et al. 2010, ApJ, 725, 36
De Breuck, C., van Breugel, W., Stanford, S. A., et al. 2002, AJ, 123, 637
Downes, D. & Solomon, P. M. 1998, ApJ, 507, 615
Drouart, G., De Breuck, C., Vernet, J., et al. 2014, A&A, 566, A53
Eales, S., Rawlings, S., Law-Green, D., Cotter, G., & Lacy, M. 1997, MNRAS, 291, 593
Emonts, B. H. C., Feain, I., Röttgering, H. J. A., et al. 2013, MNRAS, 430, 3465
Emonts, B. H. C., Norris, R. P., Feain, I., et al. 2014, MNRAS, 438, 2898
Emonts, B. H. C., Norris, R. P., Feain, I., et al. 2011, MNRAS, 415, 655
Engel, H., Tacconi, L. J., Davies, R. I., et al. 2010, ApJ, 724, 233
Greve, T. R., Ivison, R. J., & Papadopoulos, P. P. 2004, A&A, 419, 99
Hickox, R. C., Wardlow, J. L., Smail, I., et al. 2012, MNRAS, 421, 284
Ivison, R. J., Morrison, G. E., Biggs, A. D., et al. 2008, MNRAS, 390, 1117
Ivison, R. J., Smail, I., Amblard, A., et al. 2012, MNRAS, 425, 1320
Jarvis, M. J., Wilman, R. J., Röttgering, H. J. A., & Binette, L. 2003, MNRAS, 338, 263
Klamer, I. J., Ekers, R. D., Sadler, E. M., et al. 2005, ApJ, 621, L1
Lilly, S. J. & Longair, M. S. 1984, MNRAS, 211, 833
Michałowski, M. J., Dunlop, J. S., Cirasuolo, M., et al. 2012, A&A, 541, A85
Nesvadba, N. P. H., Neri, R., De Breuck, C., et al. 2009, MNRAS, 395, L16
Ogle, P., Whysong, D., & Antonucci, R. 2006, ApJ, 647, 161
Reuland, M., Röttgering, H., van Breugel, W., & De Breuck, C. 2004, MNRAS, 353, 377
Sanders, D. B., Soifer, B. T., Elias, J. H., et al. 1988, ApJ, 325, 74
Scoville, N. Z., Yun, M. S., Windhorst, R. A., Keel, W. C., & Armus, L. 1997, ApJ, 485, L21
Seymour, N., Altieri, B., De Breuck, C., et al. 2012, ApJ, 755, 146
Seymour, N., Stern, D., De Breuck, C., et al. 2007, ApJS, 171, 353
Simpson, C., Rawlings, S., Ivison, R., et al. 2012, MNRAS, 421, 3060
Tremaine, S., Gebhardt, K., Bender, R., et al. 2002, ApJ, 574, 740
Venemans, B. P., Röttgering, H. J. A., Miley, G. K., et al. 2007, A&A, 461, 823
Villar-Martín, M., Vernet, J., di Serego Alighieri, S., et al. 2003, New A Rev., 47, 291
Weilbacher, P. M., Streicher, O., Urrutia, T., et al. 2012, in Society of Photo-Optical Instrumentation Engineers (SPIE) Conference Series, Vol. 8451, Society of Photo-Optical Instrumentation Engineers (SPIE) Conference Series, 0